minerals

Article

Dioskouriite, $CaCu_4Cl_6(OH)_4 \cdot 4H_2O$: A New Mineral Description, Crystal Chemistry and Polytypism

Igor V. Pekov [1,*], Natalia V. Zubkova [1], Andrey A. Zolotarev [2], Vasiliy O. Yapaskurt [1], Sergey V. Krivovichev [2,3], Dmitry I. Belakovskiy [4], Inna Lykova [5], Marina F. Vigasina [1], Anatoly V. Kasatkin [4], Evgeny G. Sidorov [6] and Dmitry Yu. Pushcharovsky [1]

1 Faculty of Geology, Moscow State University, Vorobievy Gory, 119991 Moscow, Russia; n.v.zubkova@gmail.com (N.V.Z.); yvo72@geol.msu.ru (V.O.Y.); vigasina55@mail.ru (M.F.V.); dmitp@geol.msu.ru (D.Yu.P.)
2 Department of Crystallography, Institute of Earth Sciences, St. Petersburg State University, 199034 St Petersburg, Russia; aazolotarev@gmail.com (A.A.Z.); s.krivovichev@ksc.ru (S.V.K.)
3 Kola Science Centre, Russian Academy of Sciences, 184209 Apatity, Russia
4 Fersman Mineralogical Museum of the Russian Academy of Sciences, 119071 Moscow, Russia; dmzvr@mail.ru (D.I.B.); kasatkin@inbox.ru (A.V.K.)
5 Canadian Museum of Nature, P.O. Box 3443, Station D, Ottawa, ON K1P 6P4, Canada; ilykova@nature.ca
6 Institute of Volcanology and Seismology, Far Eastern Branch of Russian Academy of Sciences, 683006 Petropavlovsk-Kamchatsky, Russia; mineral@kscnet.ru
* Correspondence: igorpekov@mail.ru; Tel.: +7-4959394676

Abstract: A new mineral, dioskouriite, $CaCu_4Cl_6(OH)_4 \cdot 4H_2O$, represented by two polytypes, monoclinic (2*M*) and orthorhombic (2*O*), which occur together, was found in moderately hot zones of two active fumaroles, Glavnaya Tenoritovaya and Arsenatnaya, at the Second scoria cone of the Northern Breakthrough of the Great Tolbachik Fissure Eruption, Tolbachik volcano, Kamchatka, Russia. Dioskouriite seems to be a product of the interactions involving high-temperature sublimate minerals, fumarolic gas and atmospheric water vapor at temperatures not higher than 150 °C. It is associated with avdoninite, belloite, chlorothionite, eriochalcite, sylvite, halite, carnallite, mitscherlichite, chrysothallite, sanguite, romanorlovite, feodosiyite, mellizinkalite, flinteite, kainite, gypsum, sellaite and earlier hematite, tenorite and chalcocyanite in Glavnaya Tenoritovaya and with avdoninite and earlier hematite, tenorite, fluorophlogopite, diopside, clinoenstatite, sanidine, halite, aphthitalite-group sulfates, anhydrite, pseudobrookite, powellite and baryte in Arsenatnaya. Dioskouriite forms tabular, lamellar or flattened prismatic, typically sword-like crystals up to 0.01 mm × 0.04 mm × 0.1 mm combined in groups or crusts up to 1 × 2 mm^2 in area. The mineral is transparent, bright green with vitreous luster. It is brittle; cleavage is distinct. The Mohs hardness is ca. 3. D_{meas} is 2.75(1) and D_{calc} is 2.765 for dioskouriite-2*O* and 2.820 g cm^{-3} for dioskouriite-2*M*. Dioskouriite-2*O* is optically biaxial (+), α = 1.695(4), β = 1.715(8), γ = 1.750(6) and $2V_{meas.}$ = 70(10)°. The Raman spectrum is reported. The chemical composition (wt%, electron microprobe data, H_2O calculated by total difference; dioskouriite-2*O*/dioskouriite-2*M*) is: K_2O 0.03/0.21; MgO 0.08/0.47; CaO 8.99/8.60; CuO 49.24/49.06; Cl 32.53/32.66; H_2O(calc.) 16.48/16.38; -O=Cl −7.35/−7.38; total 100/100. The empirical formulae based on 14 O + Cl *apfu* are: dioskouriite-2*O*: $Ca_{1.04}(Cu_{4.02}Mg_{0.01})_{\Sigma 4.03}[Cl_{5.96}(OH)_{3.90}O_{0.14}]_{\Sigma 10} \cdot 4H_2O$; dioskouriite-2*M*: $(Ca_{1.00}K_{0.03})_{\Sigma 4.03}(Cu_{4.01}Mg_{0.08})_{\Sigma 4.09}[Cl_{5.99}(OH)_{3.83}O_{0.18}]_{\Sigma 10} \cdot 4H_2O$. Dioskouriite-2*M* has the space group $P2_1/c$, *a* = 7.2792(8), *b* = 10.3000(7), *c* = 20.758(2) Å, β = 100.238(11)°, *V* = 1531.6(2) $Å^3$ and *Z* = 4; dioskouriite-2*O*: $P2_12_12_1$, *a* = 7.3193(7), *b* = 10.3710(10), *c* = 20.560(3) Å, *V* = 1560.6(3) $Å^3$ and *Z* = 4. The crystal structure (solved from single-crystal XRD data, *R* = 0.104 and 0.081 for dioskouriite-2*M* and -2*O*, respectively) is unique. The structures of both polytypes are based upon identical **BAB** layers parallel to (001) and composed from Cu^{2+}-centered polyhedra. The core of each layer is formed by a sheet **A** of edge-sharing mixed-ligand octahedra centered by Cu(1), Cu(2), Cu(3), Cu(5) and Cu(6) atoms, whereas distorted $Cu(4)(OH)_2Cl_3$ tetragonal pyramids are attached to the **A** sheet on both sides, along with the $Ca(OH)_2(H_2O)_4Cl_2$ eight-cornered polyhedra, which provide the linkage of the two adjacent layers via long Ca−Cl bonds. The Cu(4) and Ca polyhedra form the **B** sheet. The

Citation: Pekov, I.V.; Zubkova, N.V.; Zolotarev, A.A.; Yapaskurt, V.O.; Krivovichev, S.V.; Belakovskiy, D.I.; Lykova, I.; Vigasina, M.F.; Kasatkin, A.V.; Sidorov, E.G.; et al. Dioskouriite, $CaCu_4Cl_6(OH)_4 \cdot 4H_2O$: A New Mineral Description, Crystal Chemistry and Polytypism. *Minerals* **2021**, *11*, 90. https://doi.org/10.3390/min11010090

Received: 30 December 2020
Accepted: 12 January 2021
Published: 18 January 2021

difference between the 2*M* and 2*O* polytypes arises as a result of different stacking of layers along the *c* axis. The cation array of the layer corresponds to the capped kagomé lattice that is also observed in several other natural Cu hydroxychlorides: atacamite, clinoatacamite, bobkingite and avdoninite. The mineral is named after Dioskouri, the famous inseparable twin brothers of ancient Greek mythology, Castor and Polydeuces, the same in face but different in exercises and achievements; the name is given in allusion to the existence of two polytypes that are indistinguishable in appearance but different in symmetry, unit cell configuration and XRD pattern.

Keywords: dioskouriite; calcium copper hydroxide chloride; new mineral; crystal structure; polytype; kagomé lattice; fumarole; Tolbachik volcano; Kamchatka

1. Introduction

Chlorides, oxychlorides and hydroxychlorides (hydroxide chlorides or chloride hydroxides, depending on the ratio of Cl^- and OH^- anions in a formula) of divalent copper are numerous in nature: thirty-five such minerals are known, with only atacamite, an orthorhombic $Cu_2(OH)_3Cl$, being widespread in nature, whereas others are considered as rare or extremely rare species. In this chemical family of natural compounds, thirty-one minerals contain OH or/and H_2O. The majority of the hydrogen-bearing Cu^{2+} chlorides and hydroxychlorides are supergene minerals typically formed in the oxidation zones of copper-containing ores. At the same time, there is another geological setting in which minerals containing both species-defining Cu^{2+} and Cl^- are diverse: oxidizing-type volcanic fumaroles [1,2]. Four H-free Cu^{2+} chlorides and oxychlorides are reliably known only from active fumaroles, namely tolbachite, $CuCl_2$ [3], melanothallite, Cu_2OCl_2 [4], ponomarevite, $K_4Cu_4OCl_{10}$ [5], and sanguite, $KCuCl_3$ [6]. Tolbachite, melanothallite and ponomarevite crystallize directly from gaseous phase as volcanic sublimates in the high-temperature zones (>200 °C) of fumaroles, whereas in moderately hot zones (<200 °C, mainly at 70–150 °C) of the same fumarole system, a specific copper (hydroxy)chloride mineralization is formed as a result of complex interactions between fumarole gas, atmospheric water/vapor and earlier-crystallized high-temperature minerals [2,7]. This mineral assemblage, best studied on the material from the active fumarole fields of the Tolbachik volcano, Kamchatka, Russia, includes sanguite, belloite, CuCl(OH), eriochalcite, $CuCl_2 \cdot 2H_2O$, mitscherlichite, $Cu_4Cl_6(OH)_4 \cdot 4H_2O$ [2], avdoninite, $K_2Cu_5Cl_8(OH)_4 \cdot 2H_2O$ [8,9], romanorlovite, $K_{11}Cu_9Cl_{25}(OH)_4 \cdot 2H_2O$ [10], chrysothallite, $K_6Cu_6Tl^{3+}Cl_{17}(OH)_4 \cdot H_2O$ [11], feodosiyite, $Cu_{11}Mg_2Cl_{18}(OH)_8 \cdot 16H_2O$ [12], and dioskouriite, described in this paper.

Dioskouriite, $CaCu_4Cl_6(OH)_4 \cdot 4H_2O$, is the third natural Ca-Cu hydroxychloride, after calumetite, $CaCu_4Cl_2(OH)_8 \cdot 3.5H_2O$ [13,14], and centennialite, $CaCu_3Cl_2(OH)_6 \cdot 0.7H_2O$ [13]. It is worthy to note that "vondechenite", described in 2018 as a new mineral species with the idealized formula $CaCu_4Cl_2(OH)_8 \cdot 4H_2O$ [15], was discredited in 2019 after the determination of its identity with calumetite [14].

Dioskouriite is crystallized as two polytypes, monoclinic and orthorhombic, which occur together. This feature determined the choice of its name: dioskouriite (Cyrillic: диоскурит), named after Dioskouri, the famous inseparable twin brothers of Greek mythology (in Greek, Διόσκουϱοι, which means Διός Κούϱοι, Dias or Zeus' sons), Castor and Polydeuces, the same in face but different in exercises and achievements. This alludes to the existence of two polytypes that are indistinguishable in appearance but different in symmetry, unit cell parameters and X-ray diffraction pattern in the same sample.

The new mineral, its species name dioskouriite and the names of both its polytypes, dioskouriite-2*M* for monoclinic and dioskouriite-2*O* for orthorhombic one, were approved by the IMA Commission on New Minerals, Nomenclature and Classification (IMA no. 2015–106). The names of dioskouriite polytypes are given in accord with the nomenclature of polytypes, polytypoids and polymorphs [16]. The type specimen of dioskouriite is deposited in the systematic collection of the Fersman Mineralogical Museum of the Russian Academy of Sciences, Moscow, Russia, with the catalog number 95282.

2. Occurrence and Mineral Associations

Dioskouriite was found in upper, moderately hot zones of two active fumaroles, Glavnaya Tenoritovaya (Major Tenorite) (holotype) and Arsenatnaya (cotype) situated at the Second scoria cone of the Northern Breakthrough of the Great Tolbachik Fissure Eruption 1975–1976, Tolbachik volcano, Kamchatka Peninsula, Far-Eastern Region, Russia (55°41′ N 160°14′ E, 1200 m asl). Specimens with the new mineral were collected by us in July 2014.

The Second scoria cone is a monogenetic volcano about 300 m high and 0.1 km^3 in volume formed in 1975. It is located 18 km SSW of the active volcano Ploskiy Tolbachik [17]. Both above-mentioned fumaroles occur at its summit. The Glavnaya Tenoritovaya fumarole is described in [11] and the Arsenatnaya fumarole in [18].

In Glavnaya Tenoritovaya, dioskouriite was found in sulfate-chloride incrustations and is associated with avdoninite, belloite, chlorothionite, eriochalcite, sylvite, halite, carnallite, mitscherlichite, chrysothallite, sanguite, romanorlovite, feodosiyite, mellizinkalite, flinteite, kainite, gypsum, sellaite and an incompletely studied K-Pb-Cu chloride; hematite, tenorite and chalcocyanite are earlier sublimate minerals.

In Arsenatnaya, dioskouriite and avdoninite are the latest mineral in vugs of basalt scoria altered by fumarolic gas. They are closely associated with earlier sublimate minerals: hematite, tenorite, fluorophlogopite, diopside, clinoenstatite, sanidine, halite, aphthitalite group sulfates, anhydrite, pseudobrookite, powellite and Cr^{6+}-bearing baryte.

The temperatures we measured using a chromel–alumel thermocouple in areas where the new mineral was found during its collection were 100–120 °C. Dioskouriite was probably formed not as a result of direct crystallization from a gaseous phase but as a product of the interactions involving earlier-formed high-temperature sublimate Cu- and Ca-bearing minerals, HCl-containing fumarolic gas and atmospheric components (at first, water vapor) at relatively low temperatures, presumably not higher than 120–150 °C.

3. Methods

The density of dioskouriite was measured by flotation in heavy liquids (bromoform + dimethylformamide) for the sample with the predominance of the 2*O* polytype.

The Raman spectrum of dioskouriite (sample with a mixture of both polytypes) was obtained using an EnSpectr R532 spectrophotometer (Department of Mineralogy, Moscow State University) with a green laser (532 nm) at room temperature. The output power of the laser beam on the sample was about 4 mW. The spectrum was processed in the range from 100 to 4000 cm^{-1} with the use of a holographic diffraction grating with 1800 mm^{-1} and a resolution equal to 6 cm^{-1}. The diameter of the focal spot on the sample was about 15 μm with 40x objective. The spectrum was acquired on a polycrystalline sample.

Scanning electron microscopic (SEM) studies in secondary electron (SE) mode were carried out and chemical composition was determined for all studied samples using a Jeol JSM-6480LV scanning electron microscope equipped with an INCA-Wave 500 wavelength-dispersive spectrometer (Laboratory of Analytical Techniques of High Spatial Resolution, Department of Petrology, Moscow State University), with an acceleration voltage of 20 kV, a beam current of 20 nA and a 5-μm beam diameter. H_2O was not analyzed because of the paucity of pure material.

Powder X-ray diffraction (XRD) data were collected using a Rigaku RAXIS Rapid II (X-ray Diffraction Resource Center, St. Petersburg State University, St. Petersburg, Russia) diffractometer with a curved image plate detector and a rotating anode with VariMAX microfocus optics, using Co$K\alpha$ radiation, in Debye–Scherrer geometry, at an accelerating voltage of 40 kV, a current of 15 mA and an exposure time 15 min. The distance between the sample and the detector was 127.4 mm. The data were processed using osc2xrd software [19].

Single-crystal XRD studies were carried out using a Bruker APEX II DUO diffractometer (X-ray Diffraction Resource Center, St. Petersburg State University, St. Petersburg, Russia) (2*M* polytype) and an an Oxford Diffraction SuperNova diffractometer (X-ray Diffraction Resource Center, St. Petersburg State University, St. Petersburg, Russia) (2*O* polytype), both equipped with CCD detectors (Mo*K*α radiation).

Due to the low stability of dioskouriite in moist air and its solubility in water (see below, Section 4.4), we (1) preserved the specimens by hermetic sealing and (2) prepared polished samples for electron microprobe studies using purified kerosene, without water.

4. Results

4.1. General Appearance and Physical Properties

In both fumaroles, dioskouriite occurs as well-shaped or crude crystals up to 0.01 mm × 0.04 mm × 0.1 mm in size. The crystals are tabular to lamellar, sometimes pseudo-hexagonal, or flattened prismatic, with domatic terminations that are typically sword-like (Figure 1). The crystals are combined in groups or crusts (Figures 1 and 2) up to 1 × 2 mm^2 in area and up to 0.05 mm thick, overgrowing basalt scoria or incrustations of earlier sublimate minerals covering the surface of basalt scoria.

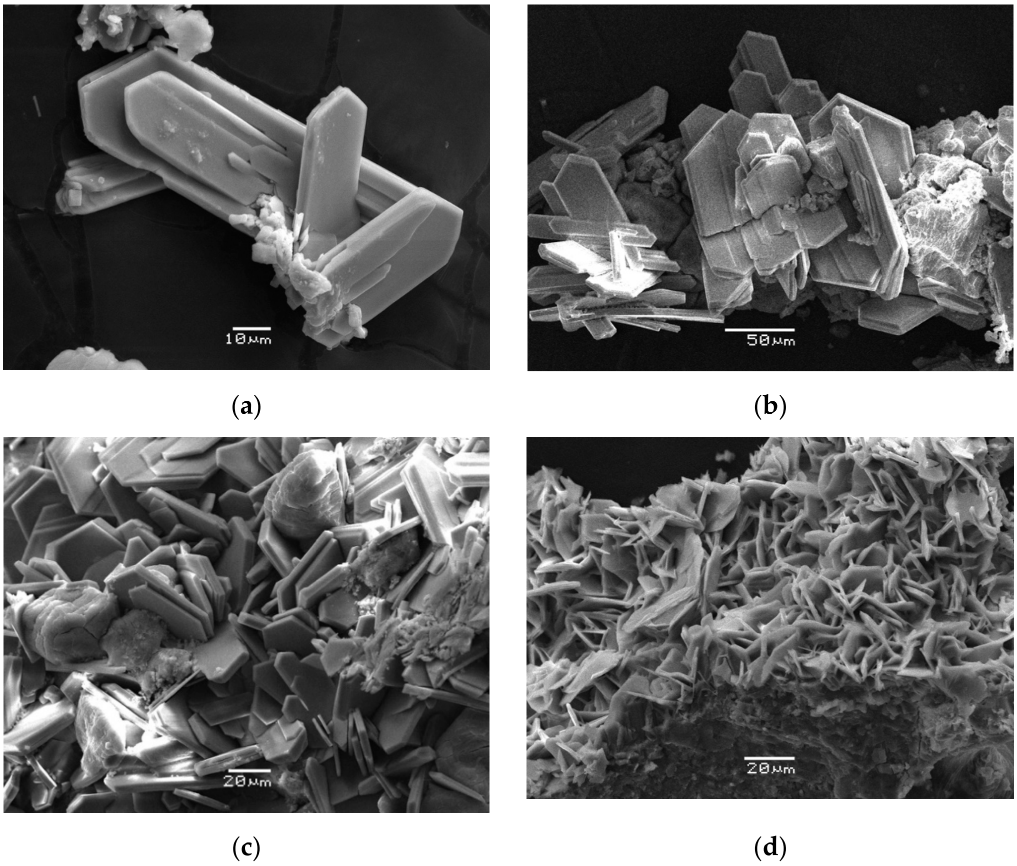

Figure 1. Morphology of dioskouriite from the Glavnaya Tenoritovaya fumarole (**a**–**c**) and from the Arsenatnaya fumarole (**d**): (**a**,**b**)—crystal groups; (**c**)—crystal crust with overgrowing crude equant crystals of carnallite; (**d**)—crystal crust overgrowing basalt scoria. SEM (secondary electron, SE) images.

Both single-crystal and powder XRD data show that the crystals of dioskouriite in both fumaroles are, in fact, parallel, syntactic intergrowths of two polytypes, 2*M* and 2*O*, in different proportions, which display considerable variations from grain to grain. In order to study each polytype, we tried to separate samples with the maximum contents of the 2*M* or 2*O* modification using XRD techniques.

Dioskouriite is transparent, bright green with light green streaks and has a vitreous luster. The mineral is brittle, with uneven fractures. One direction of distinct cleavage (assumed, based on the structure data (see below), as (001) and one direction of imperfect cleavage were observed under the microscope. The Mohs hardness is ca. 3. The measured density is 2.75(1) g cm^{-3}. Density calculated using the empirical formulae was 2.820 g cm^{-3} for dioskouriite-2*M* and 2.765 g cm^{-3} for dioskouriite-2*O*.

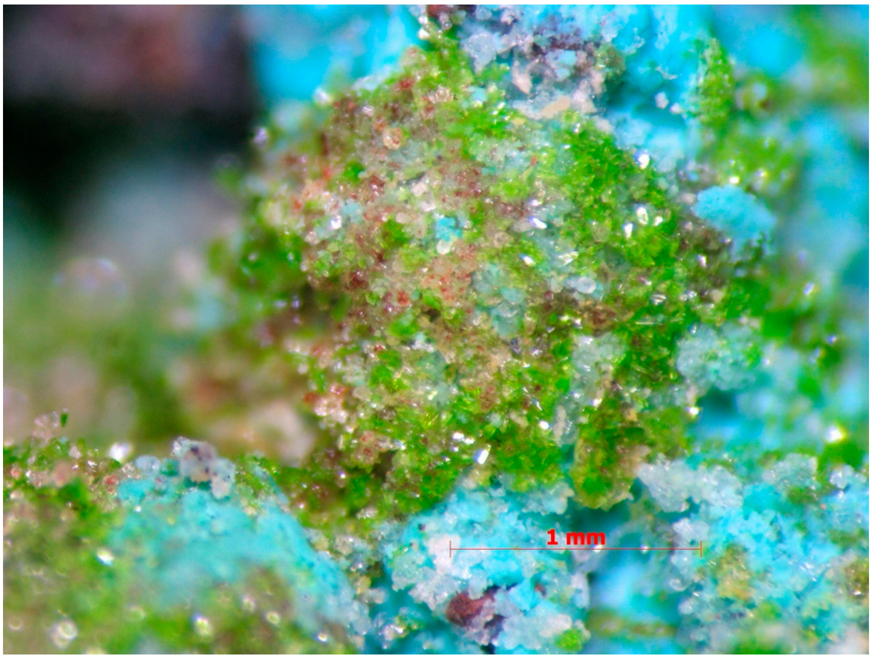

Figure 2. Crystals, crystal clusters and crusts of green dioskouriite with light blue chlorothionite and colorless carnallite and sylvite. The holotype specimen from the Glavnaya Tenoritovaya fumarole. Field of view width, 3.5 mm.

4.2. Optical Data

In plane-polarized transmitted light, dioskouriite demonstrates distinct pleochroism: *Z* (grass green) > *Y* (yellowish-green) > *X* (pale yellowish-green). The mineral is optically biaxial (+), α = 1.695(4), β = 1.715(8), γ = 1.750(6) (589 nm); $2V_{meas.}$ = 70(10)°, $2V_{calc.}$ = 75.5°. Dispersion of optical axes is very strong, $r < v$. These data were obtained for the sample with the predominant 2*O* polytype. The crystals demonstrate straight extinction parallel to the elongation.

4.3. Raman Spectroscopy

The Raman spectrum of dioskouriite is shown in Figure 3. Bands in the range from 3600 to 3200 cm^{-1} correspond to O−H stretching vibrations. We assigned the strong band with a maximum at 3460 cm^{-1} to vibrations of hydroxyl groups, whereas its distinct low-frequency shoulder with a maximum at 3380 cm^{-1} was assigned to vibrations of H_2O molecules. The band at 1590 cm^{-1} corresponds to H−O−H bending vibrations of H_2O molecules. The bands with maxima at 940, 910 and 830 cm^{-1} are assigned to O–H libration (in other terms, $Cu^{2+}\cdots$O−H bending) modes. The bands at 500 and 420 cm^{-1} correspond to Cu^{2+}−O stretching vibrations, whereas the bands with wavenumbers 300 cm^{-1} and lower can be assigned to Ca−O stretching vibrations and to lattice modes involving, in particular, Cu^{2+}−Cl and Ca−Cl vibrations.

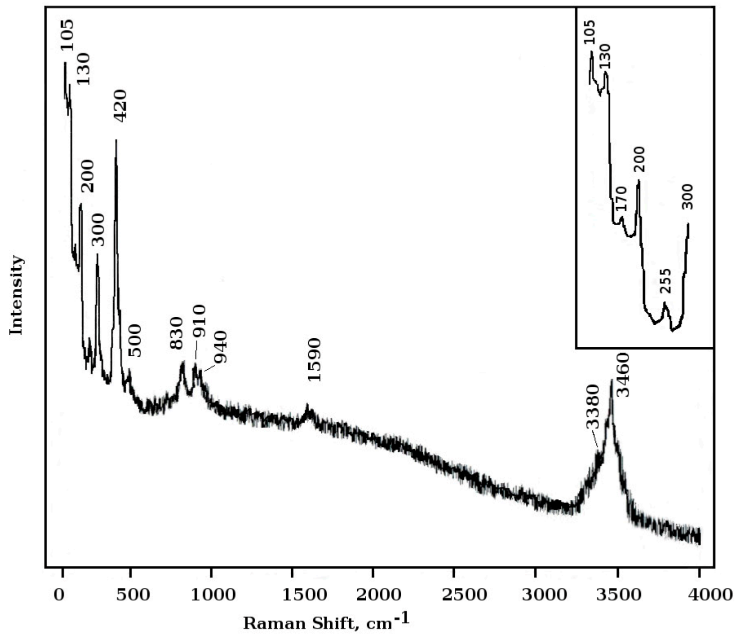

Figure 3. The Raman spectrum of dioskouriite and its enlarged low-frequency fragment.

4.4. Chemical Data

The chemical composition of both polytypes of dioskouriite is given in Table 1. Contents of other elements with atomic numbers higher than carbon are below detection limits.

Table 1. Chemical composition of dioskouriite.

Constituent	Dioskouriite-2*O*			Dioskouriite-2*M*			Probe Standard
	Wt% *	Range	SD	Wt% **	Range	SD	
K_2O	0.03	0.00–0.12	0.03	0.21	0.00–0.39	0.19	orthoclase
MgO	0.08	0.02–0.21	0.07	0.47	0.24–0.70	0.20	diopside
CaO	8.99	8.56–9.36	0.32	8.60	8.18–8.97	0.39	$CaMoO_4$
CuO	49.24	48.67–50.56	0.67	49.06	47.51–52.43	2.29	$CuFeS_2$
Cl	32.53	31.10–33.17	0.81	32.66	30.03–33.97	1.78	NaCl
H_2O_{calc} ***	(16.48)	-	-	(16.38)	-	-	-
−O=Cl	−7.35	-	-	−7.38	-	-	-
Total	100.00	-	-	100.00	-	-	-

* Averaged for six spot analyses; ** averaged for four spot analyses; *** calculated by total difference. SD—standard deviation.

The empirical formulae calculated on the basis of 14 O + Cl atoms per formula unit (*apfu*; the OH/O/H_2O ratios correspond to 4 H_2O molecules pfu) are:

1. dioskouriite-2*O*: $Ca_{1.04}(Cu_{4.02}Mg_{0.01})_{\Sigma 4.03}[Cl_{5.96}(OH)_{3.90}O_{0.14}]_{\Sigma 10}\cdot 4H_2O$;
2. dioskouriite-2*M*: $(Ca_{1.00}K_{0.03})_{\Sigma 4.03}(Cu_{4.01}Mg_{0.08})_{\Sigma 4.09}[Cl_{5.99}(OH)_{3.83}O_{0.18}]_{\Sigma 10}\cdot 4H_2O$.

The idealized, end-member formula is $CaCu_4Cl_6(OH)_4\cdot 4H_2O$, which requires CaO 8.67, CuO 49.17, Cl 32.87, H_2O 16.71, −O=Cl −7.42 and total 100 wt%.

Dioskouriite readily dissolves in H_2O at room temperature. It is unstable under room conditions and completely alters to a light blue earthy aggregate of Cu^{2+} and Ca chlorides and carbonates for several months or even days, depending on the air moisture.

4.5. X-ray Crystallography and Crystal Structure

Powder XRD data of both polytypes of dioskouriite are given in Table 2. The unit cell parameters calculated from the powder data are as follows: dioskouriite-2*M*: a = 7.291(4), b = 10.293(3), c = 20.79(1) Å, β = 100.66(5)° and V = 1533(2) Å^3; dioskouriite-2*O*: a = 7.306(2), b = 10.376(3), c = 20.62(1) Å and V = 1563(2) Å^3.

Table 2. Powder X-ray diffraction data (*d* in Å) of the two polytypes of dioskouriite.

Dioskouriite-2*M*					**Dioskouriite-2*O***				
I_{obs}	d_{obs}	I_{calc} *	d_{calc} **	*h k l*	I_{obs}	d_{obs}	I_{calc} *	d_{calc} **	*h k l*
100	**10.29**	100	10.214	002	**100**	**10.34**	100	10.280	002
3	9.26	1.5	9.197	011	2	9.28	1	9.260	011
3	7.30	3	7.252	012	3	7.32	2	7.301	012
22	**5.960**	2, 18	5.884, 5.881	−111, 110	**15**	**5.940**	7	5.980	110
7	*5.754*	0.5	5.680	013	**9**	**5.754**	11	5.742	111
11	**5.492**	5, 6	5.452, 5.444	−112, 111	-	-	-	-	-
16	**5.170**	5, 4	5.150, 5.107	020, 004	**13**	**5.177**	5, 5, 4	5.185, 5.169, 5.140	020, 112, 004
13	**5.035**	8	4.994	021	**10**	**5.033**	7	5.028	021
6	4.636	4	4.599	022	5	4.635	5	4.630	022
2	3.806	0.5	3.798	015	-	-	-	-	-
2	3.611	0.5, 1	3.626, 3.611	024, −115	2	3.601	1.5	3.603	201
1	3.555	0.5, 0.5	3.585, 3.582	−202, 200	-	-	-	-	-
4	3.418	3	3.405	006	4	3.432	2	3.427	006
5	3.300	0.5, 2	3.312, 3.254	−106, 032	4	3.282	1.5, 0.5	3.277, 3.272	032, 212
3	3.221	0.5, 3	3.213, 3.201	−204, 025	4	3.226	0.5, 4	3.228, 3.222	203, 025
2	3.151	2, 0.5	3.153, 3.147	−116, 115	-	-	-	-	-
6	3.087	1, 0.5, 3, 0.5	3.097, 3.067, 3.066, 3.062	−131, −214, 033, 212	4	3.087	2, 2, 1	3.090, 3.087, 3.082	131, 033, 213
1.5	3.043	4	3.027	131	-	-	-	-	-
4	2.982	3, 3	2.942, 2.940	−222, 220	4	2.986	4, 1.5	2.991, 2.973	132, 116
8	2.963	5, 2	2.904, 2.902	−133, 132	5	2.956	6	2.959	221
2	2.878	1, 0.5, 0.5	2.883	106	3	2.876	0.5, 0.5	2.871, 2.869	222, 034
5	*2.839*	0.5, 0.5, 0.5	2.855, 2.852, 2.849	−223, 221, 034	2	2.847	5	2.844	133
4	2.777	2.5	2.776	116	-	-	-	-	-
28	**2.737**	4, 4, 8, 7, 9, 9	2.743, 2.740, 2.726, 2.722, 2.721, 2.714	−134, 133, −224, 222, −206, 204	**21**	**2.735**	15, 16	2.740, 2.734	223, 205
2	*2.652*	0.5	2.628	035	1.5	2.671	4	2.671	134
4	2.583	2, 1.5	2.571, 2.567	−225, 223	3	2.581	3	2.585	224
3	*2.512*	0.5	2.540	027	6	2.524	3, 0.5	2.514, 2.513	042, 230
3	2.496	0.5, 3, 0.5, 0.5	2.497, 2.497, 2.480, 2.479	−231, 042, −232, 230	-	-	-	-	-
8	2.417	0.5, 0.5, 0.5, 6, 6	2.418, 2.414, 2.408, 2.406, 2.401	036, 215, 043,−226, 224	6	2.419	12	2.418	225
2	2.354	1, 1	2.346, 2.343	−234, 232	1	2.357	1	2.359	233
6	2.314	8	2.299	044	8	2.318	8	2.315	044
6	2.254	0.5, 0.5, 3	2.245, 2.242, 2.241	−235, −144, −227	5	2.253	6	2.253	226
3	2.230	3, 0.5, 0.5	2.237, 2.227, 2.226	225, 118, −218	-	-	-	-	-
1	2.193	0.5, 1	2.221, 2.178	216, 045	1.5	2.197	1	2.193	045
6	2.096	0.5, 1, 1, 4, 4	2.093, 2.0912.084, 2.080	313, −242, 240,−228, 226	5	2.097	2, 8	2.104, 2.095	241, 227
3	2.064	3	2.054	046	3	2.067	3, 0.5	2.068, 2.061	046, 218
2	1.993	1, 1	1.995, 1.980	−317, 150	1	1.986	1	1.986	151
2	1.953	1, 0.5, 1	1.962, 1.961, 1.961	−152, −333, 151	1	1.953	1, 0.5, 0.5, 1, 0.5	1.959, 1.957, 1.956, 1.952, 1.949	152, 332, 244, 316, 228
-	-	-	-	-	1	1.911	0.5, 1, 0.5	1.916, 1.914, 1.909	153, 333, 237
6	1.826	6, 0.5	1.820, 1.817	−402, −336	5	1.822	6, 2, 6	1.830, 1.825, 1.815	400, 048, 229
5	1.814	2, 3, 3	1.813, 1.806, 1.802	048, −2.2.10, 228	-	-	-	-	-
2	1.796	0.5, 1	1.792, 1.791	−404, 400	2	1.796	2, 1	1.802, 1.797	402, 238
2	*1.720*	0.5	1.716	−422	2	1.719	1, 0.5, 1	1.722, 1.719, 1.717	061, 421, 247
2	1.696	0.5, 0.5, 0.5, 0.5, 1, 1	1.693, 1.693, 1.691, 1.689, 1.686, 1.685	062, −424, 420, 342, −3.1.10, −2.2.11	2	1.698	0.5, 2	1.702, 1.694	422, 2.2.10
1	1.604	1.5	1.600	0.4.10	2	1.615	0.5, 1.5	1.614, 1.611	406, 0.4.10
-	-	-	-	-	3	1.588	1.5, 1, 0.5	1.591, 1.585, 1.580	425, 2.2.11, 350
-	-	-	-	-	2	1.526	0.5, 1.5	1.535, 1.524	0.3.12, 263
2	1.476	1, 1	1.471, 1.470	−444, 440	2	1.479	2	1.479	442
1	1.454	1, 1	1.452, 1.451	−266, 264	1	1.462	2	1.461	265
1	1.428	1.5, 1.5	1.428, 1.426	−446, 442	2	1.435	3	1.436	444
-	-	-	-	-	1	1.422	1	1.422	266
1	1.371	1, 1	1.371, 1.370	−268, 266	2	1.381	2	1.380	267
-	-	-	-	-	1	1.369	1	1.370	446
1	1.272	0.5, 0.5, 0.5, 0.5	1.277, 1.277, 1.275, 1.269	082, 0.0.16, −178, 0.4.14	1	1.292	1, 1, 1	1.296, 1.292, 1.290	080, 448, 269

* For the calculated patterns, only reflections with intensities ≥ 0.5 are given; ** for the unit cell parameters calculated from single-crystal data, the strongest reflections are marked in bold. The distinct increase, in comparison with the calculated values, in the reflections (given in italics) in the pattern of the 2*M* polytype could be caused by the admixture of the 2*O* polytype.

The structures of both polytypes of dioskouriite were studied using single crystals. The crystal structures were solved by direct methods and refined to R_1 = 0.1039 for 1805 independent reflections with $I > 2\sigma(I)$ (dioskouriite-2*M*) and to R_1 = 0.0881 for 1478 independent reflections with $I > 2\sigma(I)$ (dioskouriite-2*O*). The crystal structure refinement revealed the presence of "ghost" electron density peaks in both structure models on the *z* levels, corresponding to the positions of Cu atoms (in 2*O* polytype) and of Cu, Cl and Ca atoms (in 2*M* polytypes). The existence of these peaks was interpreted as being induced by stacking faults, i.e., by the presence of domains of another polytype in the studied crystals, as frequently observed in layered mineral structures [20,21]. Crystal data, data collection information and structure refinement details are given in Table 3, atom coordinates and displacement parameters are in Table 4a,b and Table 5a,b, selected interatomic distances are in Table 6 and the bond valence calculations are in Tables 7 and 8.

Table 3. Crystal data, data collection information and structure refinement details for dioskouriite-2*M* and dioskouriite-2*O*.

Polytype	Dioskouriite-2*M*	Dioskouriite-2*O*
Ideal formula	$CaCu_4(OH)_4Cl_6 \cdot 4H_2O$	
Ideal formula weight	647.04	
Temperature, K	293(2)	
Radiation; λ, Å	Mo*K*α; 0.71073	
Crystal system	Monoclinic	Orthorhombic
Space group; *Z*	$P2_1/c$; 4	$P2_12_12_1$; 4
Unit cell dimensions, Å,°	*a* = 7.2792(8) *b* = 10.3000(7) β = 100.238(11) *c* = 20.758(2)	*a* = 7.3193(7) *b* = 10.3710(10) *c* = 20.560(3)
V, Å^3	1531.6(2)	1560.6(3)
μ, mm^{-1}	6.881	6.752
F_{000}	1256	1256
Crystal size, mm	0.01 × 0.04 × 0.06	0.01 × 0.05 × 0.07
Diffractometer	Bruker APEX II DUO	Oxford Diffraction SuperNova
θ range, °	1.98–28.28	3.41–28.28
Index ranges	$-9 \leq h \leq 9$ $-13 \leq k \leq 13$ $-27 \leq l \leq 27$	$-5 \leq h \leq 9$ $-13 \leq k \leq 9$ $-27 \leq l \leq 27$
Reflections collected	12590	9477
Independent reflections	3846 (R_{int} = 0.1692)	3866 (R_{int} = 0.1477)
Independent reflections with $I > 2\sigma(I)$	1805	1478
Data reduction	CrysAlisPro, version 1.171.36.32 [22]	
Absorption correction	Multi-scan (empirical absorption correction using spherical harmonics, implemented in SCALE3 ABSPACK scaling algorithm)	
Structure solution	Direct methods	
Refinement method	Full-matrix least-squares on F^2	
Refined parameters *	187	201
Final *R* indices [$I > 2\sigma(I)$]	*R*1 = 0.1039, w*R*2 = 0.2574	*R*1 = 0.0881, w*R*2 = 0.2023
Goodness of Fit (GoF)	1.009	0.952
Largest difference peak and hole, e/Å^3	4.61 and −2.72	1.53 and −1.25

* The number of refined parameters is given taking into account positions of the "ghost" peaks present due to stacking faults.

Table 4. (**a**) Coordinates, equivalent displacement parameters (U_{eq}, in Å^2) of atoms and site multiplicities (Q) for dioskouriite-2*M*; **b** Residual peaks related to dioskouriite-2*O* in the difference Fourier map of dioskouriite-2*M*.

(**a**)

Atom	*x*	*y*	*z*	U_{eq}	*Q*
Cu(1)	0	0	0	0.0220(6)	2
Cu(2)	0	$\frac{1}{2}$	0	0.0251(7)	2
Cu(3)	0.7468(3)	0.25540(14)	−0.00584(9)	0.0235(5)	4
Cu(4)	0.8073(3)	0.12383(17)	0.12094(9)	0.0318(6)	4
Cu(5)	$\frac{1}{2}$	0	0	0.0215(6)	2
Cu(6)	$\frac{1}{2}$	$\frac{1}{2}$	0	0.0240(7)	2
Ca	0.6720(6)	0.4029(3)	−0.15357(17)	0.0369(9)	4
Cl(1)	0.2829(7)	0.3672(4)	0.0669(2)	0.0398(11)	4
Cl(2)	0.7835(7)	−0.1288(3)	0.0794(2)	0.0385(11)	4
Cl(3)	0.2828(6)	−0.0323(3)	0.07185(18)	0.0301(9)	4
Cl(4)	0.7867(7)	0.4496(3)	0.0775(2)	0.0376(10)	4
Cl(5)	0.0684(8)	0.1271(5)	0.1965(2)	0.0484(13)	4
Cl(6)	0.6082(7)	0.1382(4)	0.1902(2)	0.0414(11)	4
O(1)	0.9088(17)	0.3549(9)	−0.0542(5)	0.030(3)	4
O(2)	−0.0460(18)	0.1531(9)	0.0466(5)	0.032(3)	4
O(3)	0.5390(16)	0.3551(9)	−0.0547(5)	0.027(3)	4
O(4)	0.5932(18)	0.1532(8)	0.0458(5)	0.031(3)	4
O(5)	0.880(2)	0.2442(12)	−0.1875(6)	0.047(4)	4
O(6)	0.448(2)	0.2326(13)	−0.1890(7)	0.060(4)	4
O(7)	0.423(2)	0.5363(13)	−0.2071(6)	0.050(4)	4
O(8)	0.863(2)	0.5471(13)	−0.2023(7)	0.056(4)	4

(**b**)

Peak	*x*	*y*	*z*	Height (e/Å^3)
Cu(3′)	0.246(4)	0.254(2)	−0.0036(12)	1.89
Cu(4′)	0.311(5)	0.126(3)	0.1189(13)	1.62

Table 5. (**a**) Coordinates, equivalent displacement parameters (U_{eq}, in Å^2) of atoms and site multiplicities (Q) for dioskouriite-2*O*; (**b**) Residual peaks related to dioskouriite-2*M* in the difference Fourier map of dioskouriite-2*O*.

a

Site	*x*	*y*	*z*	U_{eq}	*Q*
Cu(1)	0.1262(18)	0.2504(13)	0.4997(7)	0.0205(18)	4
Cu(2)	0.6288(6)	0.7491(3)	0.5003(2)	0.0199(8)	4
Cu(3)	0.3741(4)	0.50486(19)	0.49429(12)	0.0184(5)	4
Cu(4)	0.3744(5)	0.3734(2)	0.62103(13)	0.0276(6)	4
Ca	0.3805(11)	0.6525(4)	0.3472(2)	0.0332(11)	4
Cl(1)	0.3727(9)	0.2827(4)	0.4284(3)	0.0240(11)	4
Cl(2)	0.8828(10)	0.6166(5)	0.5678(3)	0.0314(12)	4
Cl(3)	0.3772(9)	0.1219(5)	0.5792(3)	0.0280(11)	4
Cl(4)	0.3754(11)	0.7003(5)	0.5775(3)	0.0329(13)	4
Cl(5)	0.1371(10)	0.3867(6)	0.6906(3)	0.0352(13)	4
Cl(6)	0.5985(11)	0.3791(7)	0.6955(3)	0.0455(18)	4
O(1)	0.1959(18)	0.4036(13)	0.5480(8)	0.022(4)	4
O(2)	0.6915(18)	0.8965(14)	0.5564(8)	0.022(4) *	4
O(3)	0.0543(18)	0.0998(12)	0.4522(8)	0.022(4)	4
O(4)	0.5619(16)	0.6053(13)	0.4452(7)	0.017(3) *	4
O(5)	0.151(4)	0.4940(17)	0.3123(9)	0.053(6)	4
O(6)	0.594(3)	0.4842(18)	0.3109(10)	0.053(6)	4
O(7)	0.165(2)	0.7942(15)	0.2959(10)	0.041(5)	4
O(8)	0.611(3)	0.7887(17)	0.2917(9)	0.055(6)	4

* U_{iso}.

b

Peak	*x*	*y*	*z*	Height (e/Å^3)
Cu(1′)	0.609(18)	0.250(12)	0.507(7)	3.48
Cu(2′)	0.073(6)	0.749(4)	0.497(2)	3.28
Cu(3′)	0.854(2)	0.5054(14)	0.4952(8)	4.47
Cu(4′)	0.891(3)	0.3744(16)	0.6225(8)	4.12
Cl(1′)	0.851(10)	0.280(6)	0.426(3)	1.50
Cl(2′)	0.398(7)	0.612(5)	0.570(2)	1.94
Cl(3′)	0.906(7)	0.113(6)	0.578(3)	1.65
Cl(4′)	0.853(6)	0.693(4)	0.5728(18)	2.58
Ca′	0.881(8)	0.651(3)	0.3429(17)	2.38

Table 6. Selected interatomic distances (Å) in the structures of dioskouriite-2*M* and dioskouriite-2*O*.

Dioskouriite-2*M*	**Dioskouriite-2*O***
Cu(1)−O(2) 1.910(10) × 2	
−Cl(3) 2.341(4) × 2	Cu(1)−O(3) 1.915(17)
−Cl(2) 2.808(5) × 2	−O(1) 1.942(18)
	−Cl(1) 2.348(17)
Cu(2)−O(1) 1.917(9) × 2	−Cl(1) 2.397(17)
−Cl(4) 2.480(5) × 2	−Cl(3) 2.777(14)
−Cl(1) 2.651(5) × 2	−Cl(3) 2.797(14)
Cu(3)−O(3) 1.956(11)	Cu(2)−O(4) 1.936(14)
−O(1) 1.966(11)	−O(2) 1.970(15)
−O(4) 1.983(11)	−Cl(4) 2.467(9)
−O(2) 1.996(12)	−Cl(4) 2.493(9)
−Cl(4) 2.627(4)	−Cl(2) 2.673(8)
−Cl(3) 2.664(4)	−Cl(2) 2.697(8)
Cu(4)−O(4) 2.022(12)	Cu(3)−O(2) 1.980(15)
−O(2) 2.049(12)	−O(4) 1.998(14)
−Cl(6) 2.220(5)	−O(1) 2.007(14)
−Cl(5) 2.239(5)	−O(3) 2.032(14)
−Cl(2) 2.737(4)	−Cl(4) 2.652(6)
	−Cl(1) 2.672(5)
Cu(5)−O(4) 1.904(9) × 2	
−Cl(3) 2.382(4) × 2	Cu(4)−O(1) 2.015(15)
−Cl(2) 2.744(5) × 2	−O(3) 2.019(16)
	−Cl(6) 2.245(8)
Cu(6)−O(3) 1.926(10) × 2	−Cl(5) 2.255(7)
−Cl(4) 2.453(5) × 2	−Cl(3) 2.747(6)
−Cl(1) 2.660(5) × 2	
	Ca−O(7) 2.403(17)
Ca−O(8) 2.377(13)	−O(6) 2.458(18)
−O(7) 2.388(13)	−O(5) 2.46(2)
−O(5) 2.416(12)	−O(4) 2.461(15)
−O(6) 2.420(14)	−O(2) 2.469(16)
−O(3) 2.470(11)	−O(8) 2.48(2)
−O(1) 2.492(12)	−Cl(2) 2.964(7)
−Cl(1) 2.957(5)	−Cl(5) 3.248(8)
−Cl(6) 3.222(5)	

Table 7. Bond-valence calculations for dioskouriite-2*M*.

Site	Cu(1)	Cu(2)	Cu(3)	Cu(4)	Cu(5)	Cu(6)	Ca	Σ
Cl(1)	-	0.17 $^{x2\downarrow}$	-	-	-	0.17 $^{x2\downarrow}$	0.20	0.54
Cl(2)	0.11 $^{x2\downarrow}$	-	-	0.14	0.13 $^{x2\downarrow}$	-	-	0.38
Cl(3)	0.40 $^{x2\downarrow}$	-	0.17	-	0.36 $^{x2\downarrow}$	-	-	0.93
Cl(4)	-	0.27 $^{x2\downarrow}$	0.18	-	-	0.29 $^{x2\downarrow}$	-	0.74
Cl(5)	-	-	-	0.52	-	-	-	0.52
Cl(6)	-	-	-	0.55	-	-	0.10	0.65
O(1) = OH	-	0.53 $^{x2\downarrow}$	0.46	-	-	-	0.24	1.23
O(2) = OH	0.54 $^{x2\downarrow}$	-	0.42	0.37	-	-	-	1.33
O(3) = OH	-	-	0.47	-	-	0.51 $^{x2\downarrow}$	0.26	1.24
O(4) = OH	-	-	0.44	0.40	0.54 $^{x2\downarrow}$	-	-	1.38
O(5) = H_2O	-	-	-	-	-	-	0.30	0.30
O(6) = H_2O	-	-	-	-	-	-	0.29	0.29
O(7) = H_2O	-	-	-	-	-	-	0.32	0.32
O(8) = H_2O	-	-	-	-	-	-	0.33	0.33
Σ	2.10	1.94	2.14	1.98	2.06	1.94	2.04	-

Bond-valence parameters were taken from [23]. Bond-valence sums for Cl^- anions, OH^- groups and H_2O molecules do not include contributions from hydrogen bonds.

Table 8. Bond-valence calculations for dioskouriite-2*O*.

Site	Cu(1)	Cu(2)	Cu(3)	Cu(4)	Ca	Σ
Cl(1)	0.39 0.34	-	0.16	-	-	0.89
Cl(2)	-	0.16 0.15	-	-	0.20	0.51
Cl(3)	0.120.12	-	-	0.13	-	0.37
Cl(4)	-	0.280.26	0.17	-	-	0.71
Cl(5)	-	-	-	0.50	0.09	0.59
Cl(6)	-	-	-	0.52	-	0.52
O(1) = OH	0.49	-	0.41	0.40	-	1.30
O(2) = OH	-	0.46	0.44	-	0.26	1.16
O(3) = OH	0.53	-	0.39	0.40	-	1.32
O(4) = OH	-	0.50	0.42	-	0.26	1.18
O(5) = H_2O	-	-	-	-	0.26	0.26
O(6) = H_2O	-	-	-	-	0.27	0.27
O(7) = H_2O	-	-	-	-	0.31	0.31
O(8) = H_2O	-	-	-	-	0.25	0.25
Σ	1.99	1.81	1.99	1.95	1.90	-

Bond-valence parameters were taken from [23]. Bond-valence sums for Cl^- anions, OH^- groups and H_2O molecules do not include contributions from hydrogen bonds.

5. Discussion

5.1. Structure Description and Identification

Dioskouriite crystallizes as two polytypes, monoclinic and orthorhombic, with their unit cells differing from one another in the value of the β angle, which is about 100° for the monoclinic polytype (Table 3). Their crystal structures are shown in Figures 4 and 5 in polyhedral and ball-and-stick presentations, respectively. The difference between these polytypes arises as a result of different layer stacking along the *c* axis (Figure 5). The layers (see below) have identical structures and compositions in both polytypes and the mode of their interrelations is the same, which points out that in the case of dioskouriite, we observe a "classical" case of polytypism, similar to the numerous examples of layered minerals: micas, chlorites, hydrotalcite-group members, hilgardite, lamprophyllite, etc. Since both monoclinic and orthorhombic polytypes of the mineral contain two layers per unit cell, they are labeled as dioskouriite-2*M* and dioskouriite-2*O*, respectively.

There are four types of cation coordination observed in both polytypes, three for Cu^{2+} and one for Ca (see Figure 6, where each type is identified with particular crystallographic sites in both structures). The Cu atoms have a mixed-ligand coordination consisting of O and Cl atoms, previously reviewed in [24].

The first type of Cu coordination is octahedral (*Oct*1) and is composed from four Cl and two O atoms. Two Cl and two O atoms are arranged to form a (CuO_2Cl_2) square with trans-configuration of O and Cl, which is complemented by two additional Cl atoms as apices of a [(CuO_2Cl_2)Cl_2] octahedron. The octahedra are distorted due to the Jahn–Teller effect [25–27]. The distortion can be measured in terms of the difference between the <Cu−Cl_{eq}> and <Cu−Cl_{ap}> average bond lengths, $\Delta_{ap\text{-}eq}$, where Cl_{eq} and Cl_{ap} are the equatorial and apical Cl atoms, respectively. The value of $\Delta_{ap\text{-}eq}$ varies from 0.171 to 0.467 Å and is at a minimum for the Cu2 atom in the 2*M* polytype. This type of Cu coordination, [6] = [(2O + 2Cl)-*trans* + 2Cl], is typical for mixed-ligand CuO_nCl_m coordination polyhedra and has been observed in the crystal structures of avdoninite, $K_2Cu_5Cl_8(OH)_4{\cdot}2H_2O$ [9,28], melanothallite, Cu_2OCl_2 [29], and eriochalcite, $CuCl_2{\cdot}2H_2O$ [30].

The second type of Cu coordination in dioskouriite polytypes is also octahedral (*Oct*2), [6] = [(4O) + 2Cl], and consists of a planar (CuO_4) square complemented by two Cu-Cl bonds to the apical Cl atoms. This type of coordination is even more common and has been observed in the crystal structures of atacamite and clinoatacamite (two $Cu_2(OH)_3Cl$ polymorphs [31,32]), leningradite, $PbCu_3(VO_4)_2Cl_2$ [33], chloroxiphite, $Pb_3CuO_2(OH)_2Cl_2$ [34], and ilinskite, $NaCu_5O_2(SeO_3)_2Cl_3$ [24].

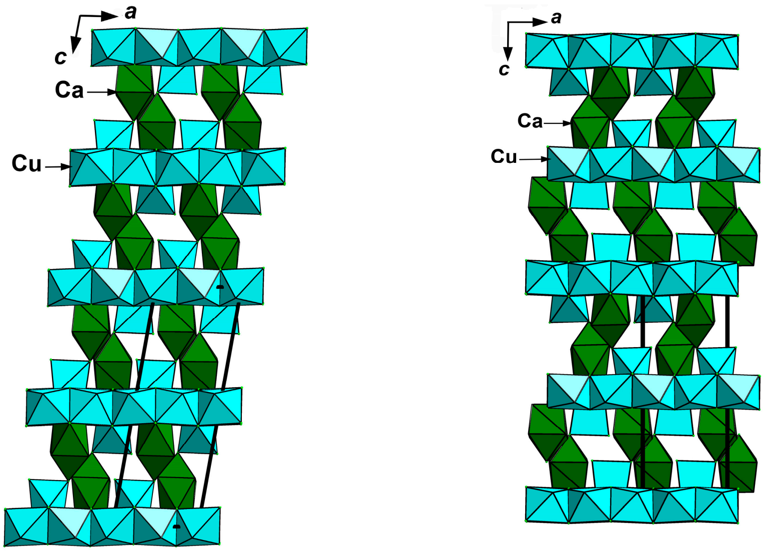

Figure 4. The crystal structures of dioskouriite-2*M* (**left drawing**) and dioskouriite-2*O* (**right drawing**) projected along the *b* axis. Only cation-centered polyhedra are shown. The unit cells are outlined.

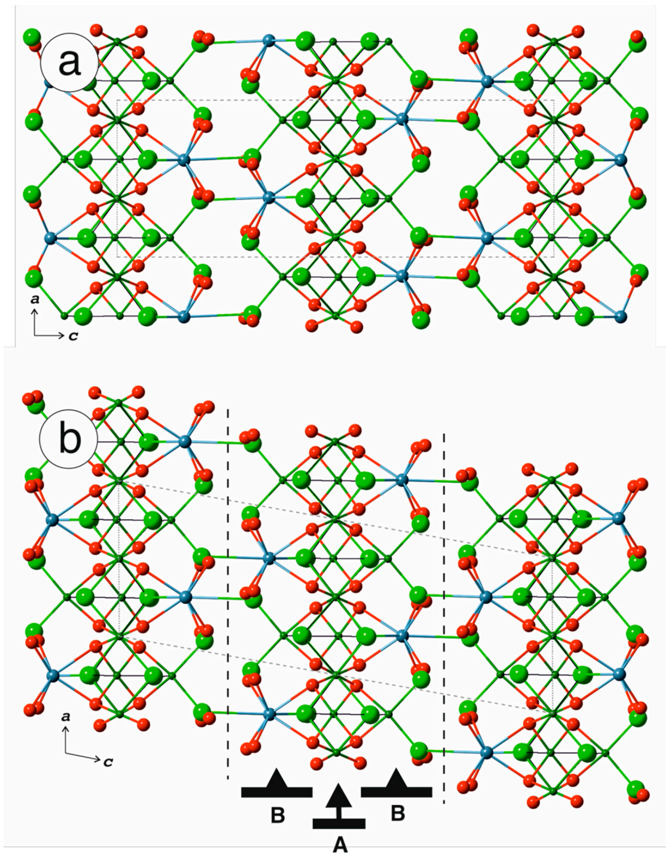

Figure 5. The layer built by Cu^{2+}-centered polyhedra with different labeling of Cu sites for dioskouriite-2*M* (**a**) and dioskouriite-2*O* (**b**). Legend: Cu, Cl, O and Ca atoms are shown as small green, large green, red and blue spheres, respectively; the Cu−Cl bonds shorter and longer than 2.5 Å are shown as dual-band cylinders and black lines, respectively.

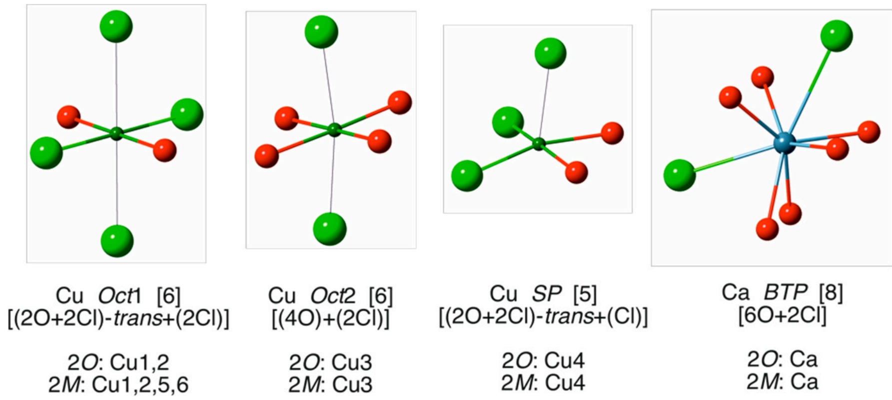

Figure 6. Four types of cation coordination in the crystal structures of dioskouriite-2*M* and dioskouriite-2*O* (see text for details). Legend as in Figure 5. *Oct*, *BTP* and *SP* mean octahedral, bicapped trigonal prismatic and (distorted) square pyramidal coordination of cation, respectively.

The third type of the Cu coordination is fivefold and can be described as distorted square pyramidal (*SP*). The base of the square pyramid is formed by two O and two Cl atoms in a cis-configuration with an additional Cl atom at the apex, [5] = [(2O + 2Cl)-*cis* + Cl]. The only other known example of such a CuO_nCl_m configuration is avdoninite, $K_2Cu_5Cl_8(OH)_4{\cdot}2H_2O$ [9,28].

There is one symmetrically independent Ca site in both structures that has an eightfold coordination that can be described as follows. The oxygen atoms of OH groups and H_2O molecules form a trigonal prism around Ca atoms with the Ca−O distances in the range from 2.377(13) to 2.492(12) Å (dioskouriite-2*M*) and from 2.403(17) to 2.48(2) Å (dioskouriite-2*O*); two Cl anions with elongated Ca−Cl distances (2.957(5) and 3.222(5) Å (dioskouriite-2*M*); 2.964(7) and 3.248(8) Å (dioskouriite-2*O*)) complete the coordination polyhedron of Ca cation. The geometry of this coordination can therefore be described as bicapped trigonal prismatic (*BTP*), which is one of the three most common eightfold coordinations known in inorganic chemistry, along with dodecahedral and square antiprismatic coordinations [35].

The crystal structures of both polytypes are based upon complex layers of ca. 1-nm thickness. The layers are stacked along the *c* axis and can be considered as built up from the sheets of the two types, **A** and **B,** with the **A** sheet sandwiched between two **B** sheets, so the layers have the formula **BAB**.

The projections of the **A** and **B** sheets are shown in Figure 7.

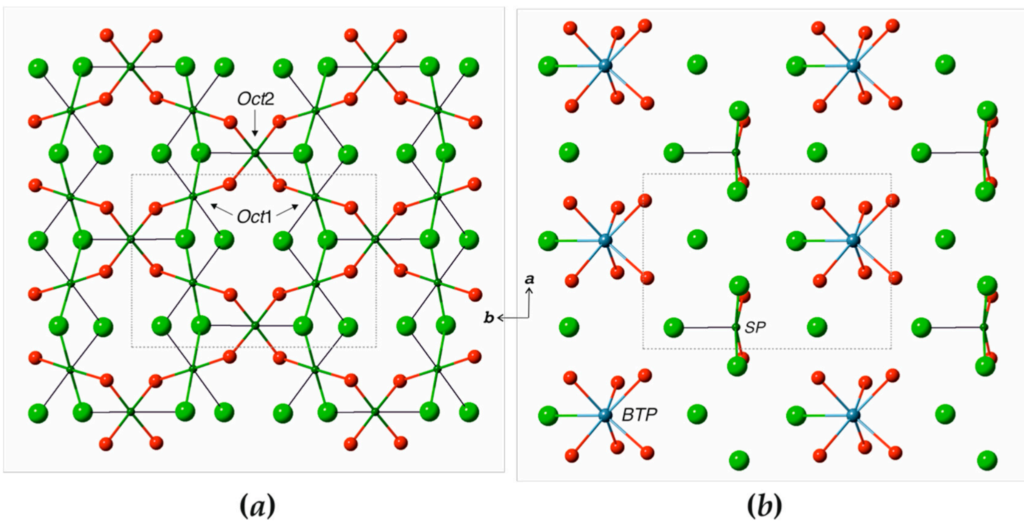

Figure 7. The projections of the **A** (**a**) and **B** (**b**) sheets in the crystal structure of dioskouriite-2*O* along the *c* axis. Legend as in Figures 5 and 6.

The **A** sheet, which is at the core of the **BAB** layer, is constructed as follows. The *Oct*1 octahedra share their trans $Cu_{eq}-Cu_{ap}$ edges to form chains running parallel to the *a* axis (Figure 7a). The chains are linked via *Oct*2 octahedra that share four of their $O_{eq}-Cl_{ap}$ edges with adjacent *Oct*1 octahedra so that sheets are formed. The **B** sheets contain isolated *BTP* and *SP* polyhedra (Figure 7b) that are attached to the **A** sheet via Cu−OH, Ca−OH, Cu−Cl and Ca−Cl bonds.

The linkage of the **BAB** layers is provided by the long Ca−Cl bonds oriented approximately perpendicular to the plane of the layers (Figure 5).

The 2*M* and 2*O* polytypes of dioskouriite can be easily distinguished from one another using powder XRD data. The most reliable diagnostic sign is the presence of relatively strong reflections with $d \approx 5.4$–5.5 Å in the powder XRD pattern of dioskouriite-2*M* (the −112 and 111 reflections with close *d* values that can appear as a singlet in the measured XRD diagram), which are absent in the XRD pattern of dioskouriite-2*O* (Table 2).

The high values of a crystallographic agreement factor *R* (10.39% for dioskouriite-2*M* and 8.81% for dioskouriite-2*O*) are due to the stacking faults, which reflect the occurrence of both polytypes in the same crystal. Analysis of residual electron density peaks in different Fourier syntheses indicated that the two strongest peaks for dioskouriite-2*M* (Table 4b) and the nine strongest peaks for dioskouriite-2*O* (Table 5b) correspond to the positions of the Ca and Cu atoms when the layers are shifted relative to each other by $a/2$. The residual electron density peaks observed for the 2*O* polytype approximately correspond to the cation positions of the 2*M* polytype and vice versa. Both 2*M* and 2*O* polytypes are maximum degree of order (MDO) polytypes, which are the simplest of the possible ordered sequences and usually correspond to the most frequently occurring polytypes in the family [36].

5.2. Relations to Other Species

The crystal structures of dioskouriite polytypes are related to the structures of minerals and synthetic inorganic compounds consisting of layers based upon Cu^{2+} cation arrays with a capped kagomé geometry. The latter is one of the most common cationic patterns in Cu oxysalts that possess interesting magnetic properties such as a spin-liquid state [37–43]. From a geometrical point of view, a kagomé net is a tiling of a plane consisting of regular triangles and hexagons (Figure 8). In the capped kagomé pattern, each triangle is capped either from above or below by an additional node, so each triangle in the plane forms the basis of a regular tetrahedron oriented either up or down relative to the plane of the net. In most of the structures, the kagomé pattern is distorted, i.e., the ideal hexagonal geometry of the net is violated. Among Cu hydroxychlorides, a distorted kagomé geometry has been observed in atacamite and clinoatacamite, $Cu_2(OH)_3Cl$ [32,44], bobkingite, $Cu_5(OH)_8Cl_2 \cdot 2H_2O$ [45], and avdoninite, $K_2Cu_5Cl_8(OH)_4 \cdot 2H_2O$ [9,28]. The capped kagomé geometry can be derived from the cristobalite- or pyrochlore-type arrangement of Cu atoms observed in atacamite and clinoatacamite [44], as shown in Figure 8. The Cu array in these two $Cu_2(OH)_3Cl$ polymorphs can be described as a framework of corner-sharing "empty" Cu_4 tetrahedra (Figure 8a). Cutting it into layers along the (011) plane in atacamite results in the formation of a 2D layer with a capped kagomé geometry (Figure 8b,c), i.e., a planar arrangement of Cu atoms with all triangles capped by additional Cu atoms located on both sides of the sheet. In all the minerals mentioned above, except for the dioskouriite polytypes, the arrays are homometallic, i.e., they are composed of Cu atoms only. In contrast, the cationic array of the **BAB** layer in dioskouriite consists of Cu and Ca atoms, where half of the triangles are capped by Ca.

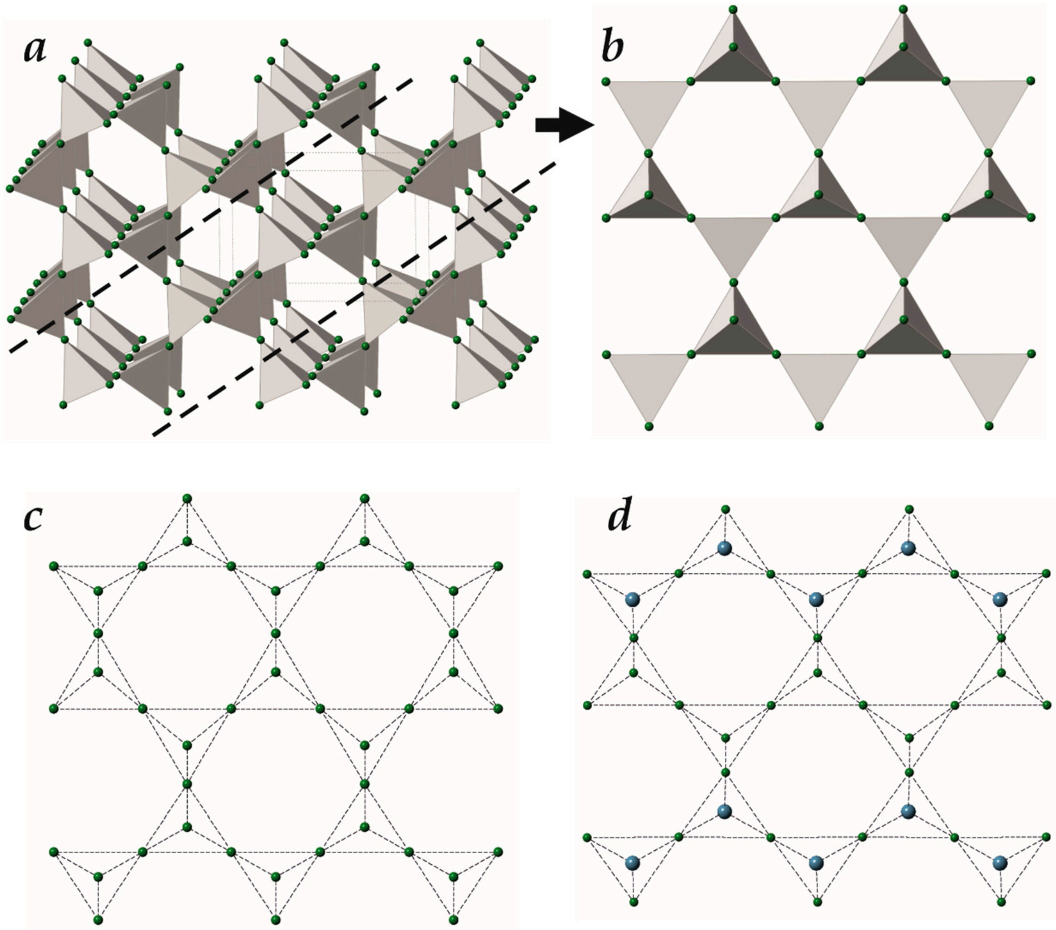

Figure 8. The array of Cu atoms shown as a cristobalite- or pyrochlore-like framework of corner-sharing Cu_4 tetrahedra (**a**); the sheet excised from the framework along the plane indicated by striated line as shown in **a** (**b**); the ball-and-stick representation of the 2D Cu-capped kagomé array in atacamite (**c**) and the 2D Cu-Ca array in dioskouriite polytype (**d**).

In the real structures of the Cu hydroxychloride minerals, the capped kagomé arrays are decorated by Cl atoms and (OH) groups and the modes of the decoration differ from structure to structure. Figure 9 shows the ball-and-stick representations of the **A**-type layers in atacamite, clinoatacamite, bobkingite and avdoninite. In all cases, the topology of the interatomic linkage is the same and the layers have the overall formula [$Cu_3\phi_8$], where ϕ = Cl, OH. In the crystal structures of atacamite, clinoatacamite and bobkingite, the stoichiometry of the layers is [$Cu_3(OH)_6Cl_2$], whereas the crystal structures of avdoninite and dioskouriite polytypes are based upon the [$Cu_3(OH)_4Cl_4$] layers. Ideally, the layers with different Cl−OH arrangements can be described using idealized diagrams, shown in Figure 10. Figure 10a shows an ideal geometry, whereas Figure 10a–e provide the schemes of distribution of Cl and OH over anionic sublattices in different minerals. The deviations from the ideal geometry due to the different sizes of Cl^- and $(OH)^-$ anions may be essential, as can be seen in Figure 9.

The topological relations between the crystal structures of dioskouriite and other natural Cu hydroxychlorides indicate the energetical stability of the kagomé geometry. The kagomé arrays in dioskouriite polytypes are distorted and therefore less interesting from the viewpoint of their magnetic properties. Nevertheless, it is worthy of investigation, which needs a pure synthetic material. Since no artificial analogs of dioskouriite have been reported so far, its synthesis may be a reasonable task.

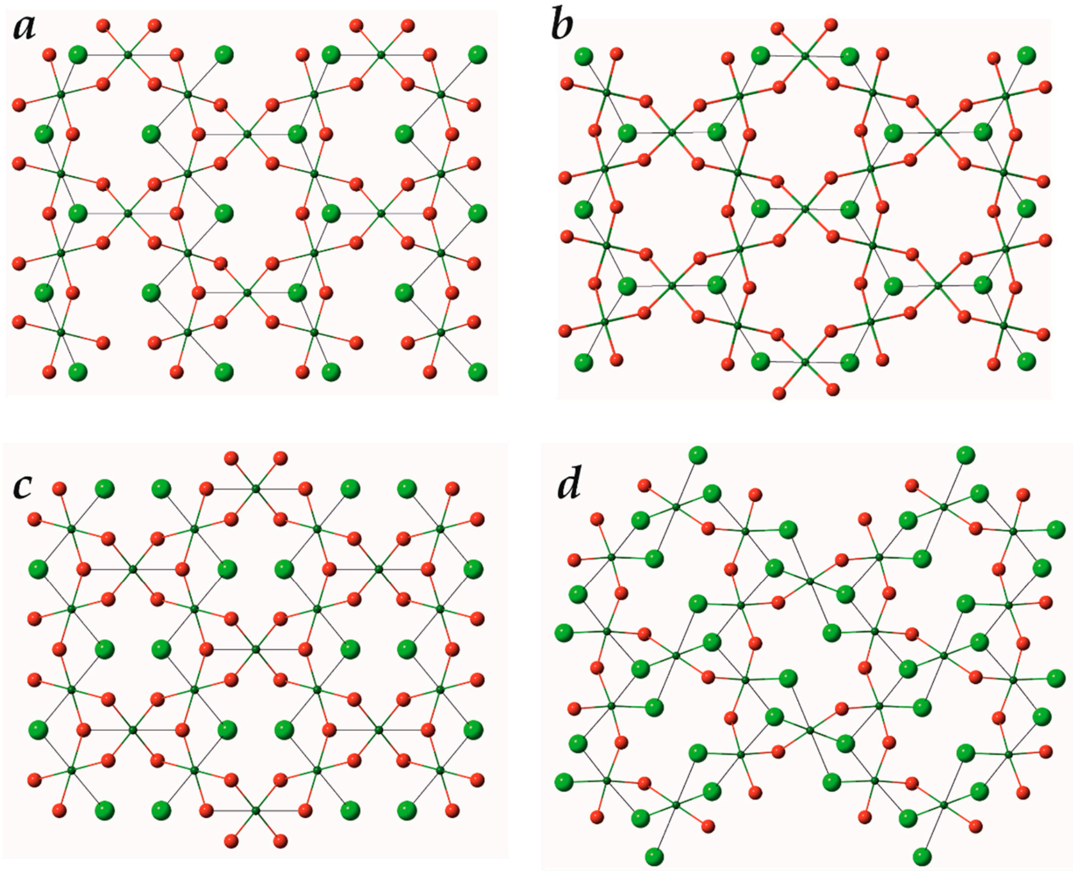

Figure 9. The $[Cu_3\phi_8]$ layers (ϕ = Cl, OH) in the crystal structures of atacamite (parallel to (011) (**a**); clinoatacamite (parallel to (011) (**b**); bobkingite (parallel to (001) (**c**) and avdoninite (parallel to (100) (**d**). Legend as in Figure 5.

5.3. Structural Complexity and Relative Stability

The structural complexity of the two polytypes has been estimated using the information-based parameters elaborated in [46,47] and taking into account the H-correction [48]. Both crystal structures belong to the category of complex structures (500–1000 bit/cell), with dioskouriite-2*M* being slightly more complex (5.019 bit/atom and 622.230 bit/cell) than dioskouriite-2*O* (4.954 bit/atom and 614.320 bit/cell). The information densities for the 2*M* and 2*O* polytypes are equal to 0.406 and 0.394 bit/$Å^3$, respectively. The difference in information density correlates well with the difference in physical densities—2.820 and 2.765 g/cm^3, respectively. This allows to consider the 2*O* polytype as being slightly less stable (or metastable) compared to the 2*M* polytype. One may also consider the 2*O* polytype as a high-temperature phase and the 2*M* polytype as a low-temperature phase. The same kind of relation has been observed in a number of minerals and inorganic compounds: the metastable high-temperature polymorph possessing lower density and lower complexity compared to the stable low-temperature polymorph (see [46] and [49] for a recent discussion of the topic). However, there are very small doubts that both polytypes are energetically close to each other and that this causes their common formation and the presence of domains of both polytypes in the same crystals. The existence of stacking faults and intimate intergrowths of the two polytypes may indicate the oscillating temperature and/or kinetic regime of crystallization of the mineral inside volcanic fumaroles.

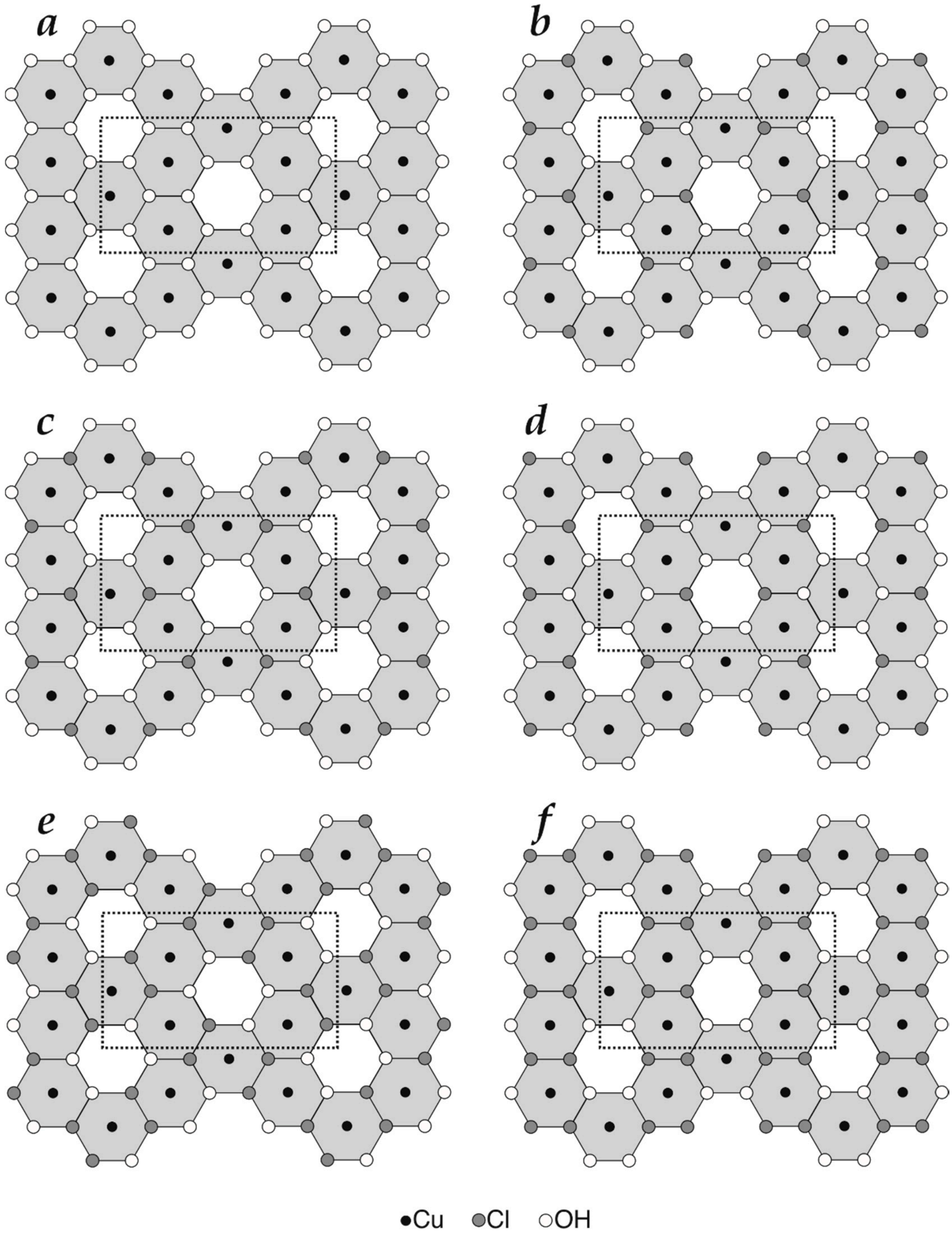

Figure 10. The idealized model of the [$Cu_3\phi_8$] layer (ϕ = Cl, OH) (**a**) and the schemes of the OH/Cl population in the crystal structures of atacamite (**b**), clinoatacamite (**c**), bobkingite (**d**), avdoninite (**e**) and dioskouriite polytypes (**f**).

Author Contributions: I.V.P., N.V.Z. and S.V.K. wrote the paper. V.O.Y. and A.V.K. obtained and processed the chemical data. A.A.Z. obtained and processed the single-crystal XRD data. I.V.P. and A.A.Z. obtained and processed the powder XRD data. N.V.Z., A.A.Z. and S.V.K. studied the crystal structures. S.V.K. and D.Yu.P. performed the crystal chemical analysis. I.V.P., I.L. and E.G.S. collected the material and prepared it for laboratory studies. D.I.B. obtained the optical characteristics. M.F.V. obtained and processed the Raman spectrum. I.L. measured density. All authors have read and agreed to the published version of the manuscript.

Funding: This work was supported by the Russian Science Foundation, grant no. 19-17-00050.

Institutional Review Board Statement: Not applicable.

Informed Consent Statement: Not applicable.

Data Availability Statement: Not applicable.

Acknowledgments: We are grateful to two anonymous referees and the Academic Editor for their useful comments. We thank the X-ray Diffraction Resource Center of St. Petersburg State University for providing instrumental and computational resources.

Conflicts of Interest: The authors declare no conflict of interest.

References

1. Vergasova, L.P.; Filatov, S.K. A study of volcanogenic exhalation mineralization. *J. Volcanol. Seismol.* **2016**, *10*, 71–85. [CrossRef]
2. Pekov, I.V.; Zubkova, N.V.; Pushcharovsky, D.Y. Copper minerals from volcanic exhalations—a unique family of natural compounds: Crystal chemical review. *Acta Crystallogr.* **2018**, *B74*, 502–518. [CrossRef]
3. Vergasova, L.P.; Filatov, S.K. A new mineral, tolbachite, $CuCl_2$. *Dokl. Akad. Nauk SSSR* **1983**, *270*, 415–417. (In Russian) [CrossRef]
4. Vergasova, L.P.; Filatov, S.K. Chemical formula and crystal chemical characterization of melanothallite, Cu_2OCl_2. *Zapiski RMO* **1982**, *124*, 562–565. (In Russian)
5. Vergasova, L.P.; Filatov, S.K.; Serafimova, E.K.; Semenova, T.F. Ponomarevite, $K_4Cu_4OCl_{10}$, a new mineral from volcanic exhalations. *Dokl. Akad. Nauk SSSR* **1988**, *300*, 1197–1200. (In Russian)
6. Pekov, I.V.; Zubkova, N.V.; Belakovskiy, D.I.; Lykova, I.S.; Yapaskurt, V.O.; Vigasina, M.F.; Sidorov, E.G.; Pushcharovsky, D.Y. Sanguite, $KCuCl_3$, a new mineral from the Tolbachik volcano, Kamchatka, Russia. *Can. Miner.* **2015**, *53*, 633–641. [CrossRef]
7. Pekov, I.V.; Agakhanov, A.A.; Zubkova, N.V.; Koshlyakova, N.V.; Shchipalkina, N.V.; Sandalov, F.D.; Yapaskurt, V.O.; Turchkova, A.G.; Sidorov, E.G. Oxidizing-type fumaroles of the Tolbachik Volcano, a mineralogical and geochemical unique. *Russ. Geol. Geophys.* **2020**, *61*, 675–688.
8. Chukanov, N.V.; Murashko, M.N.; Zadov, A.E.; Bushmakin, A.F. Avdoninite, $K_2Cu_5Cl_8(OH)_4 \cdot H_2O$, a new mineral from volcanic exhalations and from the zone of technogenesis at massive sulfide ore deposits. *Zapiski RMO* **2006**, *148*, 38–42. (In Russian)
9. Pekov, I.V.; Krivovichev, S.V.; Chukanov, N.V.; Yapaskurt, V.O.; Sidorov, E.G. Avdoninite: New data, crystal structure and refined formula $K_2Cu_5Cl_8(OH)_4 \cdot 2H_2O$. *Geol. Ore Dep.* **2016**, *58*, 568–578. [CrossRef]
10. Pekov, I.V.; Yapaskurt, V.O.; Britvin, S.N.; Vigasina, M.F.; Lykova, I.S.; Zubkova, N.V.; Krivovichev, S.V.; Sidorov, E.G. Romanorlovite, a new copper and potassium hydroxychloride from the Tolbachik volcano, Kamchatka, Russia. *Geol. Ore Depos.* **2017**, *59*, 601–608. [CrossRef]
11. Pekov, I.V.; Zubkova, N.V.; Belakovskiy, D.I.; Yapaskurt, V.O.; Vigasina, M.F.; Lykova, I.S.; Sidorov, E.G.; Pushcharovsky, D.Y. Chrysothallite $K_6Cu_6Tl^{3+}Cl_{17}(OH)_4 \cdot H_2O$, a new mineral species from the Tolbachik volcano, Kamchatka, Russia. *Miner. Mag.* **2015**, *79*, 365–376. [CrossRef]
12. Pekov, I.V.; Zubkova, N.V.; Yapaskurt, V.O.; Belakovskiy, D.I.; Lykova, I.S.; Vigasina, M.F.; Ksenofontov, D.A.; Britvin, S.N.; Sidorov, E.G.; Khanin, D.A.; et al. Feodosiyite, $Cu_{11}Mg_2Cl_{18}(OH)_8 \cdot 16H_2O$, a new mineral from the Tolbachik volcano, Kamchatka, Russia. *N. Jb. Miner. Abh.* **2018**, *195*, 27–39. [CrossRef] [PubMed]
13. Crichton, W.; Müller, H. Centennialite, $CaCu_3(OH)_6Cl_2.nH_2O$, n = 0.7, a new kapellasite-like species, and a reassessment of calumetite. *Mineral. Mag.* **2016**, *81*, 1105–1124. [CrossRef]
14. Miyawaki, R.; Hatert, F.; Pasero, M.; Mills, S.J. New minerals and nomenclature modifications approved in 2019. IMA Commission on New Minerals, Nomenclature and Classification (CNMNC), Newsletter 49. *Mineral. Mag.* **2019**, *83*, 479–483. [CrossRef]
15. Schlüter, J.; Malcherek, T.; Pohl, D.; Schäfer, C. Vondechenite, a new hydrous calcium copper chloride hydroxide, from the Bellerberg, East-Eifel volcanic area, Germany. *N. Jb. Mineral. Abh.* **2018**, *195*, 79–86. [CrossRef]
16. Nickel, E.H.; Grice, J.D. The IMA Commission on New Minerals and Mineral Names: Procedures and guidelines on mineral nomenclature. *Can. Miner.* **1998**, *36*, 913–926.
17. Fedotov, S.A.; Markhinin, Y.K. (Eds.) *The Great Tolbachik Fissure Eruption*; Cambridge University Press: New York, NY, USA, 1983.
18. Pekov, I.V.; Koshlyakova, N.N.; Zubkova, N.V.; Lykova, I.S.; Britvin, S.N.; Yapaskurt, V.O.; Agakhanov, A.A.; Shchipalkina, N.V.; Turchkova, A.G.; Sidorov, E.G. Fumarolic arsenates—A special type of arsenic mineralization. *Eur. J. Mineral.* **2018**, *30*, 305–322. [CrossRef]
19. Britvin, S.N.; Dolivo-Dobrovolsky, D.V.; Krzhizhanovskaya, M.G. Software for processing the X-ray powder diffraction data obtained from the curved image plate detector of Rigaku RAXIS Rapid II diffractometer. *Zap. Ross. Mineral. Obsh.* **2017**, *146*, 104–107. (In Russian)
20. Krivovichev, S.V.; Armbruster, T.; Yakovenchuk, V.N.; Pakhomovsky, Y.A.; Men'shikov, Y.P. Crystal structures of lamprophyllite-2M and lamprophyllite-2O from the Lovozero alkaline massif, Kola peninsula, Russia. *Eur. J. Mineral.* **2003**, *15*, 711–718. [CrossRef]
21. Yakovenchuk, V.N.; Krivovichev, S.V.; Ivanyuk, G.Y.; Pakhomovsky, Y.A.; Selivanova, E.A.; Zhitova, E.A.; Kalashnikova, G.O.; Zolotarev, A.A.; Mikhailova, J.A.; Kadyrova, G.I. Kihlmanite-(Ce), $Ce_2TiO_2[SiO_4](HCO_3)_2(H_2O)$, a new rare-earth mineral from the pegmatites of the Khibiny alkaline massif, Kola Peninsula, Russia. *Mineral. Mag.* **2014**, *78*, 483–496. [CrossRef]
22. Agilent. *CrysAlis PRO*; Agilent Technologies UK Ltd.: Yarnton, UK, 2013.

23. Brese, N.E.; O'Keeffe, M. Bond-valence parameters for solids. *Acta Crystallogr.* **1991**, *47*, 192–197. [CrossRef]
24. Krivovichev, S.V.; Filatov, S.K.; Vergasova, L.P. The crystal structure of ilinskite, $NaCu_5O_2(SeO_3)_2Cl_3$, and review of mixed-ligand CuOmCln coordination geometries in minerals and inorganic compounds. *Miner. Petrol.* **2013**, *107*, 235–242. [CrossRef]
25. Jahn, H.A.; Teller, E. Stability of polyatomic molecules in degenerate electronic states. I. Orbital degeneracy. *Proc. R. Soc.* **1937**, *A161*, 220–235.
26. Hathaway, B.J. Copper. In *Comprehensive Coordination Chemistry*; Pergamon, G.W., Ed.; Oxford: Oxford, UK, 1987; Volume 5, pp. 533–774.
27. Burns, P.C.; Hawthorne, F.C. Mixed-ligand $Cu^{2+}\Phi_6$ octahedra in minerals: Observed stereochemistries and Hartree-Fock calculations. *Can. Mineral.* **1995**, *33*, 1177–1188.
28. Kahlenberg, V. On the crystal structure of $K_2Cu_5Cl_8(OH)_4{\cdot}2(H_2O)$. *Z. Anorg. Allg. Chem.* **2004**, *630*, 900–903. [CrossRef]
29. Krivovichev, S.V.; Filatov, S.K.; Burns, P.C. The cuprite-like framework of OCu_4 tetrahedra in the crystal structure of synthetic melanothallite, Cu_2OCl_2, and its negative thermal expansion. *Can. Mineral.* **2002**, *40*, 1185–1190. [CrossRef]
30. Brownstein, S.; Han, N.F.; Gabe, E.J.; le Page, Y. A redetermination of the crystal structure of cupric chloride dihydrate. *Z. Kristallogr.* **1989**, *189*, 13–15. [CrossRef]
31. Parise, J.B.; Hyde, B.G. The structure of atacamite and its relationships to spinel. *Acta Crystallogr.* **1986**, *B42*, 1277–1280. [CrossRef]
32. Malcherek, T.; Schlueter, J. Structures of the pseudo-trigonal polymorphs of $Cu_2(OH)_3Cl$. *Acta Crystallogr.* **2009**, *B65*, 334–341. [CrossRef]
33. Siidra, O.I.; Krivovichev, S.V.; Armbruster, T.; Filatov, S.K.; Pekov, I.V. The crystal structure of leningradite, $PbCu_3(VO_4)_2Cl_2$. *Can. Mineral.* **2007**, *45*, 445–449. [CrossRef]
34. Siidra, O.I.; Krivovichev, S.V.; Turner, R.W.; Rumsey, M.S. Chloroxiphite $Pb_3CuO_2(OH)_2Cl_2$: Structure refinement and description of oxocentred OPb_4 tetrahedra. *Mineral. Mag.* **2008**, *72*, 793–798. [CrossRef]
35. Burdett, J.K.; Hoffmann, R.; Fay, R.C. Eight-Coordination. *Inorg. Chem.* **1978**, *17*, 2553–2568. [CrossRef]
36. Merlino, S.; Perchiazzi, N.; Franco, D. Brochantite, $Cu_4SO_4(OH)_6$: OD character, polytypism and crystal structures. *Eur. J. Mineral.* **2003**, *15*, 267–275. [CrossRef]
37. Han, T.-H.; Singleton, J.; Schlueter, J.A. Barlowite: A spin-1212 antiferromagnet with a geometrically perfect kagome motif. *Phys. Rev. Lett.* **2014**, *113*, 227203. [CrossRef] [PubMed]
38. Norman, M.R. Herbertsmithite and the search for the quantum spin liquid. *Rev. Mod. Phys.* **2016**, *88*, 041002. [CrossRef]
39. Malcherek, T.; Mihailova, B.; Welch, M.D. Structural phase transitions of clinoatacamite and the dynamic Jahn-Teller effect. *Phys. Chem. Miner.* **2017**, *44*, 307–321. [CrossRef]
40. Malcherek, T.; Welch, M.D.; Williams, P.A. The atacamite family of minerals—A testbed for quantum spin liquids. *Acta Crystallogr.* **2018**, *B74*, 519–526. [CrossRef]
41. Siidra, O.; Nazarchuk, E.; Agakhanov, A.; Polekhovsky, Y. Aleutite $[Cu_5O_2](AsO_4)(VO_4){\cdot}(Cu_{0.5}\square_{0.5})Cl$, a new complex salt-inclusion mineral with Cu^{2+} substructure derived from a Kagome-net. *Mineral. Mag.* **2019**, *83*, 847–853. [CrossRef]
42. Smaha, R.W.; He, W.; Jiang, J.M. Materializing rival ground states in the barlowite family of kagome magnets: Quantum spin liquid, spin ordered, and valence bond crystal states. *NPJ Quantum Mater.* **2020**, *5*, 23. [CrossRef]
43. Hiroi, Z.; Ishikawa, H.; Yoshida, H.; Yamaura, J.; Okamoto, Y. Orbital transitions and frustrated magnetism in the kagome-type copper mineral volborthite. *Inorg. Chem.* **2019**, *58*, 11949–11960. [CrossRef]
44. Krivovichev, S.V.; Hawthorne, F.C.; Williams, P.A. Structural complexity and crystallization: The Ostwald sequence of phases in the $Cu_2(OH)_3Cl$ system (botallackite–atacamite–clinoatacamite). *Struct. Chem.* **2017**, *28*, 153–159. [CrossRef]
45. Hawthorne, F.C.; Cooper, M.A.; Grice, J.D.; Roberts, A.C.; Hubbard, N. Description and crystal structure of bobkingite, ${Cu^{2+}}_5Cl_2(OH)_8(H_2O)_2$, a new mineral from New Cliffe Hill Quarry, Stanton-under-Bardon, Leicestershire, UK. *Mineral. Mag.* **2002**, *66*, 301–311. [CrossRef]
46. Krivovichev, S.V. Structural complexity of minerals: Information storage and processing in the mineral world. *Mineral. Mag.* **2013**, *77*, 275–326. [CrossRef]
47. Krivovichev, S.V. Which inorganic structures are the most complex? *Angew. Chem. Int. Ed.* **2014**, *53*, 654–661. [CrossRef]
48. Krivovichev, S.V.; Krivovichev, V.G.; Hazen, R.M. Structural and chemical complexity of minerals: Correlations and time evolution. *Eur. J. Mineral.* **2018**, *30*, 231–236. [CrossRef]
49. Kolitsch, U.; Weil, M.; Kovrugin, V.; Krivovichev, S. Crystal chemistry of the variscite and metavariscite groups: Crystal structures of synthetic $CrAsO_4{\cdot}2H_2O$, $TlPO_4{\cdot}2H_2O$, $MnSeO_4{\cdot}2H_2O$, $CdSeO_4{\cdot}2H_2O$ and natural bonacinaite, $ScAsO_4{\cdot}2H_2O$. *Mineral. Mag.* **2020**, *84*, 568–583. [CrossRef]